Pd-Decorated CuO Thin Film for Photodegradation of Acetaminophen and Triclosan under Visible Light Irradiation

Citation: Katal, Reza, Panah, Saeid Masudy, Saeedikhani, Mohsen, Kosari, Mohammadreza, Sheng, Chua Chin et al. 2018. "Pd-Decorated CuO Thin Film for Photodegradation of Acetaminophen and Triclosan under Visible Light Irradiation." Advanced Materials Interfaces, 5 (24).

As Published: http://dx.doi.org/10.1002/admi.201801440

Publisher: Wiley

Persistent URL: https://hdl.handle.net/1721.1/140789

Version: Author's final manuscript: final author's manuscript post peer review, without publisher's formatting or copy editing

Pd Decorated CuO Thin Film for Photodegradation of Acetaminophen and Triclosan under Visible Light Irradiation

Reza Katal,[a,#] Saeid Masudy Panah,[b,c,#] Mohsen Saeedikhani,[d] Mohammadreza Kosari,[e] Chua Chin Sheng,[f] Ong Say Leong,[a] Gong Xiao,*[,b,c] Hu Jiangyong*[,a]

[a] Department of Civil & Environmental Engineering, National University of Singapore, Engineering Drive 2, Singapore 117576

[b] Department of Electrical and Computer Engineering, National University of Singapore, Singapore 119260

[c] Low Energy Electronic System (LEES), Singapore-MIT Alliance for Research and Technology (SMART), 1 CREATE Way, #09-01/02 CREATE Tower, Singapore 138602

[d] Department of Materials Science and Engineering, National University of Singapore, Singapore 117583.

[e] Department of Chemical and biomolecular Engineering, National University of Singapore, Singapore 117585

[f] Institute of Materials Research and Engineering, A*STAR (Agency for Science, Technology and Research), 2 Fusionopolis Way. Innovis, #08-03, Singapore 138634.

* Corresponding author:

Dr. Gong Xiao, **Email:** elegong@nus.edu.sg , **Tel:** (+65) 65167871

Prof. Hu Jiangyong, **Email:** ceehujy@nus.edu.sg , **Tel:** (+65) 6516 4540

 # These authors contributed equally.

Abstract: Inefficient visible light photocatalytic degradation of organic pollutants, such as Acetaminophen (ACE) and Triclosan (TS), is one of the main limiting factors for implementing cost-effective metal oxide photocatalyst for large-scale deployment. Here, we develop a highly efficient CuO thin film photocatalyst through rapid thermal annealing. The CuO thin film was decorated with Pd nanostructures for enhanced visible light degradation of ACE and TS. It is shown that compared to the as-deposited thin CuO film photocatalyst, the rapid thermal assisted CuO (A-CuO) photocatalyst can significantly enhance charge generation and separation efficiency through improvement of crystallinity and reduction of recombination centres. Furthermore, it is demonstrated that the incorporation of Pd nanostructures could considerably increase optical absorption, which further improve the photocatalytic performance through the enhancement of surface plasmon resonance (SPR). The CuO film with the 40s of Pd sputtering (Pd40-CuO) showed the highest performance for photocatalytic degradation of both ACE and TS. The Pd40-CuO film showed good stability and did not show any considerable reduction in photocatalytic activity after 5 cycles. This indicated the high potential of Pd40-CuO for water and wastewater treatment in industrial scale.

Keyword: CuO thin film, Pd nanostructures, photocatalytic, visible light

1. Introduction

In recent decades, concern about rising the concentration of organic pollutants such as pharmaceutical and personal care products (PPCPs) and pesticides in different types of water resources have widely increased. The organic pollutants are detected in different types of wastewater (municipal and industrial)[1–3] and surface and groundwater [4,5]. The biodegradability of PPCPs are low and conventional water and wastewater treatment is not effective for removing these pollutants. Various kind of oxidation processes are used for destruction of PPCPs compounds in the aqueous media [6–8]. Due to difficulties in degrading PPCPs, they are considered a serious threat to public health and aquatic ecosystem [9–12].

UV/H_2O_2 treatment [13,14], ozonation [15], Fenton/photo-Fenton oxidation [16,17], heterogeneous catalytic oxidation with H_2O_2 [18], and heterogeneous photocatalytic process[19,20] have been widely used for the degradation of organic pollutants. Among these processes, heterogeneous photocatalytic process is considered as a suitable strategy for removal of the organic pollutants from aqueous environment due to the durability, ease of application and maintenance, nontoxic products and reusability of photocatalyst [21-26].

Based on fascinating physical and chemical features of transition metal oxide, these materials are widely used in different fields and industries. Due to availability, non-toxicity and high optical absorption in visible light range, copper oxide is identified as promising candidate for photocathode manufacturing [21,22]. The two common types of the copper oxides are CuO (cupric oxide) and Cu_2O (Cupric cuprous). Cu_2O is a direct gap semiconductor with optical band gap of 2.1–2.6 eV., while CuO is an indirect gap semiconductor with lower band gap energy of 1.2–1.6 eV. The lower band gap energy makes CuO a suitable candidate for application in photocatalytic processes under visible light [27-30].

Various methods such as electrochemical deposition, evaporation, sputtering and thermal oxidation has been employed for the CuO thin film deposition[31-34]. Among them, Sputtering method provides the following advantages: (a) simplicity, (b) reproducibility of the film properties and (c) controlling the film's microstructure and its thickness by adjusting the sputtering conditions [35-37]. Several studies indicate that plasmonic nanostructures can promote the performance of the photocatalyst under visible light illumination [38,39]. Plasmonic photocatalysis are prepared by dispersing noble metal (Au, Ag, Pd, Pt) nanoparticles into semiconductor photocatalysts. Plasmonic photocatalysis forms a Schottky junction with the photocatalyst, resulting in localized surface plasmonic resonance (LSPR) effect. The LSPR improves the photocatalytic activity through generation of more active charge carriers and enhancing charge separation [39]. Some noble metal-semiconductor composite were prepared and used for the photocatalytic process to improve the photocatalytic activity [38-39].

In this paper, a highly efficient and stable CuO thin film photocatalyst was developed by reducing recombination centers and improving optical absorption over wide range of spectra through crystal engineering and incorporating Pd plasmonic nanostructures. The prepared samples were used as photocatalyst for degradation of acetaminophen (ACE) and triclosan (TS) in aqueous solution under visible light irradiation. Pd sputtered in 40 s on the annealed CuO thin film (Pd40-CuO) sample showed the best performance among the prepared photocatalysts. Most of the synthesized or commercial photocatalysts are in powder form and the main challenge for their application in large scale is theirs recovery and separation from aqueous media. In this study, by deposition of CuO thin film on the substrate, we could overcome this challenge. For the first time, the mechanism of organic pollutants degradation by CuO thin film was comprehensively studied. The identification of

intermediates for both contaminants during the photocatalytic reaction was also investigated. The influence of radical trappers on the photocatalytic degradation of the ACE and TS by Pd40–CuO was also investigated. These results showed that ·OH, $\cdot O_2^-$ (or $^1O_2$) radicals did not play an important role in degradation of the TS and their generations were not as the rate-limiting step for TS photocatalytic degradation. It was found that CuO pathway for degradation of pollutants was different. For the first time, we found that for degradation of ACE, the main procedure is oxidation; but for TS, initial procedure is reduction (dechlorinating) followed by oxidation. The photocatalysts stability and recycling are the two important parameters for application of them in industrial scale. In this study, the recycling and stability of photocatalysts for ACE and TS photocatalytic degradation were comprehensively investigated. AsD showed the poor stability and a considerable amount of the CuO thin film departed from the substrate. The stability of A-CuO and Pd40-CuO was much better than AsD and lower amount of CuO film departing from the substrate was observed.

2. Results and discussion

2.1. Characterization

Fig. 1 shows the powder X-ray diffraction (XRD) patterns of AsD, A-CuO and Pd60-CuO. The XRD peaks of the substrate was removed from XRD spectra. As can be seen, all samples have two distinct peaks at 2-theta value of 35.482 ((002) plane) and 38.764 ((111) plane) degree (JCPDS# 05-0661) [36]. The corresponding full width half maximum (FWHM) of the XRD peaks are calculated and presented in Fig. 1a; by annealing of the samples (A-CuO and Pd60-CuO), the XRD peaks become intense and value of FWHM decreases [36]. This illustrates that a better crystallinity was obtained by annealing of samples [36]. The

corresponding crystallite size of the main XRD peak of CuO (111) for AsD and annealed samples (A-CuO and Pd60-CuO) were determined from the Scherrer formula, $D = K\lambda/\beta \cos\theta$, where D, K, λ, β and θ are grain size, dimensionless shape factor, X-ray wavelength, line broadening at FWHM in radians and Bragg angle, respectively. Fig. 1b indicates the crystallite size of samples before (AsD) and after (A-CuO and Pd60-CuO) annealing; as shown, annealing of samples leads to a larger size of crystallite.

Distinct surface morphology was observed in FESEM images of AsD and rapid thermal annealed CuO films (A-CuO) (Fig. 2). The AsD CuO films had very smooth surface formed with uniform nano-sized crystallites (less than 20 nm). Annealing at 550 $^{\circ}$C, induce roughness on the film surface and the grain size was surprisingly increased (more than 100 nm) and grain boundaries became very prominent. Thus, FESEM analysis validates our XRD results and endorses that grain size was increased and crystalline property improved after thermal treatment.

The SEM and corresponding elemental mapping analyses were conducted to investigate the morphology of Pd40-CuO as indicated in Fig. S1. From Fig. S1a, it is difficult to distinguish the Pd and CuO thin film in the low resolution SEM. The EDX spectrum of the Pd40-CuO (Fig. S1b) exhibits the presence of signals of C, Cu, O and Pd elements. The mapping results of the Fig. S1a (selected zone) are shown in Fig. S1c–e in which the distributions of Cu and O elements are the very same. It clearly presents that Pd element is uniformly dispersed on the surface of CuO thin film. The weight percentage of elemental Cu, O and Pd were 40.7, 39.7, and 19.6, respectively.

Fig. S2 shows the FESEM of A-CuO before doping and after of Pd sputtering at various times (20, 40 and 60s). As can be seen, by increasing the sputtering time, concentration of Pd

in the surface of the samples clearly increased. It clearly presents that Pd element is uniformly dispersed on the surface of CuO thin film.

To evaluate the Pd distribution on the surface of CuO thin film, top view TEM image of Pd40-CuO was taken and presented in the Fig. S3. It shows that Pd element is uniformly distributed on the surface of thin film. To measure the thickness of the CuO thin film, the cross sectional TEM image of Pd40-CuO is taken and presented in Fig. S4. As shown, the thickness of CuO thin film is around 500 nm.

To evaluate the chemical state of samples, the X-ray photoelectron spectroscopy (XPS) analysis are shown in Fig. 3. As shown, peaks of C 1s, Cu 2p and O 1s are recorded and shown in Fig. 3a. The peak of Pd 3d is just recorded and shown in Fig. 3a for Pd-CuO sample; other samples (AsD and A-CuO) did not show this peak that proves the existence of Pd in Pd-CuO sample. XPS signals from the Cu 2p region of AsD, A-CuO and Pd60-CuO are indicated in Fig. 3b. The peaks at 935.60 eV and 955.60 eV were ascribed to the core levels of Cu $2p_{3/2}$ and Cu $2p_{1/2}$, respectively [40, 41]. The appearance of O 1s region peak at 530.60 eV hinted the presence of crystal lattice oxygen in the samples (Fig.3c) [42]. The peaks at 335.6 eV and 340.6.10 eV (Pd60-CuO) were related to the core levels of Pd $3d_{5/2}$ and Pd $3d_{3/2}$, respectively (Fig. 3d) [43, 44]. According to Fig. 3b, Shake-up features at 940-945 and 960-965 eV for the Cu $2p_{3/2}$ and $2p_{1/2}$ core levels are evident and diagnostic of an open 3d9 shell of Cu(+2). The peak positions and relative intensities of the satellites from these levels are indicative of the presence of CuO at the surface [45-47].

2.2. **Photocatalytic degradation of ACE and TS**

Photocatalytic activities of photocatalysts (As-Deposited, A-CuO, Pd20-CuO, Pd40-CuO and Pd60-CuO) were investigated by degradation of ACE and TS in aqueous solution

under visible light (>420 nm) illumination. As shown in Fig. 4a & b, Pd40-CuO exhibited superior visible light activity for photodegradation of ACE and TS in comparison with other photocatalysts. Only 32% ACE and 79% TS were photodegraded by A-CuO after 4 hours, while near 70% ACE and 99% TS were degraded by using Pd40-CuO, indicating an improvement in photocatalytic performance. By comparison of photocatalytic performance of the As-Deposited and A-CuO, the results also showed that heat treatment (annealing) improved the photocatalytic activity of CuO film. The k_{app} values for ACE and TS degradation are presented in Table 1. As shown, Pd40-CuO shows the highest photodegradation rate, which is much higher than that of A-CuO and As-deposited. As can be seen, by increasing the sputtering time up to 40s, the photocatalytic degradation efficiency of ACE and TS was increased but after this time, a reduction was observed. This phenomenon can be explained in this way that if the amount of Pd in photocatalyst is lower than optimum, less electrons will be transferred; it is also possible that more holes and electrons pair recombination take place. At higher sputtering time (>optimum), the Pd can also act as a shield for photocatalyst in front of irradiation and decrease the quantum efficiency [48].

The photocurrent is commonly considered as an important standard to examine the separation performance of photogenerated h^+ and e^- pairs and the photocatalytic activity of photocatalysts [48]. The photocurrent responses of Pd40-CuO, A-CuO and AsD samples are presented in Fig. 5 under visible light irradiation. An improvement in photocurrent density demonstrated the enhancement in separation efficiency of the photogenerated h^+ and e^- pair, which is suitable for photocatalytic and photoelectrochemical activity [41, 49]. The photocurrent density of A-CuO was 80 μA cm^{-2}. After sputtering of Pd, the photocurrent densities was raised to 180 μA cm^{-2} which demonstrated the considerable role of Pd in generation and separation of h^+ and e^- pair. By sputtering of Pd on the CuO thin film,

absorption of visible light was also improved and this consequently raised the efficiency of photogenerated e^- and h^+ pair under visible light illumination (Fig. 6); enabling more electrons for reaction with electron acceptors in aqueous phase.

Fig. 7 shows the influence of radical trappers on the degradation of the ACE and TS by Pd40–CuO. The ethanol [50], sodium azide [51,52] and hydrogen peroxide [53] were applied as the radical trappers for $^{\cdot}OH$, $^{\cdot}O_2^-$ (or $^1O_2$), and electrons, respectively. The concentrations of ethanol, sodium azide and hydrogen peroxide in aqueous solution were 5 mmol L^{-1}. As can be seen, the ethanol and sodium azide increased the photocatalytic degradation rate of TS by Pd40–CuO but addition of H_2O_2 showed the negative effect on the TS photocatalytic degradation rate. The same results were also reported by other researchers [41]. These results showed that $^{\cdot}OH$, $^{\cdot}O_2^-$ (or $^1O_2$) radicals did not play an important role in photocatalytic degradation of the TS and their generations were not as the rate-limiting step for TS photodegradation. By contrast, hydrogen peroxide that acted as an electron trapper, reduced the TS photocatalytic degradation rate; this results indicated that electron generation was the key step in the TS photocatalytic degradation by Pd40–CuO. Addition of ethanol obviously reduced the photocatalytic degradation rate of ACE but for sodium azide, this reduction was lower than ethanol. Hydrogen peroxide also improved the ACE photocatalytic degradation rate. These results showed that $^{\cdot}OH$ radicals played an important role in photocatalytic degradation of the ACE and their generations were as the rate-limiting step for ACE photocatalytic degradation. It found that for degradation of ACE, the main procedure is oxidation; but for TS, initial procedure is reduction (dechlorinating) followed by oxidation. As shown, Pd40–CuO exhibited superior performance for TS photocatalytic degradation (reduction) and it can be also concluded that this photocatalyst is more suitable for photoreduction reaction of organic pollutant.

2.3. **Photocatalyst stability and Recycling**

The photocatalysts stability and recycling are the two important parameters for application of them in industrial scale. In this study, the recycling and stability of photocatalysts for ACE and TS photocatalytic degradation were investigated and presented in Fig. 8 a & b, respectively. After each cycle, the electrodes were washed with acetone and water for removal of the adsorbates. As can be seen, photocatalytic degradation percentage of the A-CuO and Pd40-CuO after 5 cycles did not significantly change. For the A-CuO, the photocatalytic degradation percentage was reduced by less than 6 %; for Pd40-CuO, this reduction was less than 4%. FE-SEM images of the all electrodes after (five cycles) and before using in photocatalytic reactions are presented in Fig. 9. As can be seen, AsD showed the poor stability and a considerable amount of the CuO thin film departed from the substrate. The stability of the A-CuO and Pd40-CuO was much better than AsD and lower amount of the CuO film departed from substrate. The FESEM images (higher resolution) of fresh Pd40-CuO and used one (after using 5 cycles for photocatalytic degradation) are shown in Fig. S5. As can be seen, sputtered Pd showed considerable stability after 5 cycles and did not depart from the surface of the thin film.

3. Conclusion

In this paper, highly efficient and stable thin CuO film photocatalyst was developed by reducing recombination centers and improving optical absorption over wide range of spectra through crystal engineering and incorporating Pd plasmonic nanostructures. The samples was used as photocatalyst for degradation of ACE and TS in aqueous solution under visible light irradiation. Pd40-CuO showed the best performance among the photocatalysts. The influence of radical trappers on the photocatalytic degradation of the ACE and TS by Pd40–CuO is also investigated. These results showed that ·OH, $^{\cdot}O_2^-$ (or $^1O_2$) radicals did not play an important role in degradation of the TS and their generations were not as the rate-limiting step for TS photocatalytic degradation. Generally, photocatalysts showed the better performance for degradation of TS. Furthermore, it was shown that photocatalytic degradation percentage of the A-CuO600 and Pd40-CuO photocatalyst after 5 cycles does not significantly change indicating significant improvement of stability. FE-SEM images showed that for As-deposited sample, considerable amount of the CuO thin film departed from the substrate while much lower amount of CuO film separated from substrate for A-CuO and Pd40-CuO samples.

4. Experimental

4.1. Materials and instruments

All chemical reagents were of high purity and were used as received from Sigma–Aldrich–Fluka (Singapore). A Milli-Q water purification system (Millipore Synergy 185, US) provided the water used for all solutions and suspensions. The Field Emission Scanning Electron Microscopy (FESEM) was used for the investigation of the sample morphology (FEI

Verios 460 FESEM). The purity and crystalline structure of the samples was also examined by a bruker D-8 general area detector XRD system (GADDS) in θ–2θ scan using a CuKα (ʎ= 0.15418 nm) radiation. X-ray photoelectron spectroscopy (XPS, AXIS ULTRA) by a monochromatic Al Kα X-ray source was utilized for the analysis of the surface. To determine the organic pollutants concentrations, a HPLC (Agilent; column, ZORBAX Eclipse XDBC18, 4.6 mm× 150 mm, 5 µm) was utilized with a flow rate of 1.0 mL/min and UV absorbance detection at 242 nm.

4.2. CuO thin film and Pd sputtering

CuO thin film was sputtered onto FTO coated glass substrate. Before the deposition process, the FTO glass were ultra-sonicated in IPA for 10 min and then dried by blowing nitrogen gas. Stoichiometric CuO target and radio frequency (RF) sputtering system were used for deposition of CuO thin film on the substrate. The sputtering power, the evacuation pressure and working pressure were 100 W, 3×10^{-4} mTorr and 3.3 mTorr, respectively. The deposited CuO films were annealed in 550 $^{\circ}$C (A-CuO) in nitrogen atmosphere for 1 min using the rapid thermal annealing (RTA) system. Heating and cooling rates of RTA system were 15 $^{\circ}$C s^{-1} and 10 $^{\circ}$C s^{-1}, respectively. The Pd nanostructures were formed on A-CuO thin films by depositing of Pd at sputtering power of 25 W in 3 different sputtering times of 20s (Pd20-CuO), 40s (Pd40-CuO) and 60s (Pd60-CuO).

4.3. Photocatalytic experiments

CuO thin film deposited on the FTO coated glass surface were used as photocatalyst for batch experiments (Fig. S6). CuO samples after annealing were cut into cube with length, width and height of 15, 15 and 1 mm and then placed at the bottom of the beaker. Next, 20 mL of 10.0 mg L^{-1} ACE or TS solution was mixed in the beaker. Then the beaker was placed on the shaker (50 rpm, ambient temperature) for 30 min in the dark. For the photocatalytic

experiments, a xenon arc lamp (150 W) with a 400 nm cut off filter was put at 100 mm above the solution for visible light illumination. After photocatalytic degradation experiments in required time, a 2 mL sample of each experiments were sampled and their concentration were analyzed. The equation 1 was used for determination of ACE and TS photocatalytic degradation rate (%) from aqueous solution:

$$\text{Photocatalytic degradation rate (\%)} = \frac{C_o - C_t}{C_0} \times 100 \quad (1)$$

Where C_o is the initial pollutant concentration and C_t is the pollutant concentration at time t in the solution. The L-H model was used to describe the kinetic of pollutants degradation under visible light illumination:

$$r = -\frac{dC}{dt} = \frac{k_r KC}{1+KC} \quad (2)$$

Where r, C and t are the rate of the destruction of pollutant, the concentration of solution and reaction time, respectively. K and k_r represent the equilibrium constant for sorption of pollutant and the limiting rate constant of the reaction under the experimental conditions, respectively. At low concentration, KC value is much lower than 1 and this term can be neglected in equation 2. By neglecting this term, the equation 2 can be converted to a first-order kinetics model (eq. 3):

$$r = -\frac{dC}{dt} = k_r KC = k_{app} C \quad (3)$$

The k_{app} is the apparent first-order rate constant. By integrating from Eq. (3) and using boundary condition $C = C_o$ at $t = 0$ gives:

$$\ln\left(\frac{C_t}{C_o}\right) = -k_{app} t \quad (4)$$

In Eq. 4, C_o is the pollutants initial concentration in aqueous solution.

Photo-generated currents of samples were measured using a 0.1 M Na_2SO_4 electrolyte. A bias voltage of 0.1 V was applied for photo-generated currents measurement in presence and absence (dark condition) of visible light illumination.

Conflicts of interest

There are no conflicts to declare.

Acknowledgments

The authors acknowledge the financial support from the Singapore International Graduate Award (SINGA).

References

[1] M. Carballa, F. Omil, J. M. Lema, M. Llompart, C. García-Jares, I. Rodríguez, M. Gómez, T. Ternes, *Water Res.* **2004**, *38*, 2918.

[2] Q. Cai, J. Hu, *J. Hazard. Mater.* **2017**, *323*, 527.

[3] S. Li, J. Hu, *J. Hazard. Mater.* **2016**, *318*, 134.

[4] P. E. Stackelberg, E. T. Furlong, M. T. Meyer, S. D. Zaugg, A. K. Henderson, D. B. Reissman, *Sci. Total Environ.* **2004**, *329*, 99.

[5] B. T. Huy, C. T. B. Thao, V-D. Dao, N. T. K. Phuong, Y-I. Lee, *Adv. Mater. Interf* **2017**, *4*, 1700128.

[6] D. Stülten, S. Zühlke, M. Lamshöft, M. Spiteller, *Sci. Total Environ.* **2008**, *405*, 310.

[7] Z.-T. Hu, Z. Chen, R. Goei, W. Wu, T.-T. Lim, *Nanoscale* **2016**, *8*, 12736.

[8] Q. Wang, J. Huang, H. Sun, K.-Q. Zhang, Y. Lai, *Nanoscale* **2017**, *9*, 16046.

[9] Y. Sun, B. Qu, Q. Liu, S. Gao, Z. Yan, W. Yan, B. Pan, S. Wei, Y. Xie, *Nanoscale* **2012**, *4*, 3761.

[10] C.-T. Chang, J.-J. Wang, T. Ouyang, Q. Zhang, Y.-H. Jing, *Mater. Sci. Eng. B* **2015**, *196*, 53.

[11] K. Sun, L. Wang, C. Wu, J. Deng, K. Pan, *Adv. Mater. Interf.* **2017**, *4*, 1700845.

[12] K. Kümmerer, *Chemosphere* **2001**, *45*, 957.

[13] M. Klavarioti, D. Mantzavinos, D. Kassinos, *Environ. Int.* **2009**, *35*, 402.

[14] I. Kim, N. Yamashita, H. Tanaka, *J. Hazard. Mater.* **2009**, *166*, 1134.

[15] D. Vogna, R. Marotta, A. Napolitano, R. Andreozzi, M. D'Ischia, *Water Res.* **2004**, *38*, 414.

[16] N. Klamerth, L. Rizzo, S. Malato, M. I. Maldonado, A. Agüera, A. R. Fernández-Alba, *Water Res.* **2010**, *44*, 545.

[17] L. A. Pérez-Estrada, M. I. Maldonado, W. Gernjak, A. Agüera, A. R. Fernández-Alba, M. M. Ballesteros, S. Malato, *Catal. Today* **2005**, *101*, 219.

[18] J. Hofmann, U. Freier, M. Wecks, S. Hohmann, *Appl. Catal. B Environ.* **2007**, *70*, 447.

[19] P. CALZA, V. SAKKAS, C. MEDANA, C. BAIOCCHI, A. DIMOU, E. PELIZZETTI, T. ALBANIS, *Appl. Catal. B Environ.* **2006**, *67*, 197.

[20] L. Rizzo, S. Meric, D. Kassinos, M. Guida, F. Russo, V. Belgiorno, *Water Res.* **2009**, *43*, 979.

[21] A. Paracchino, V. Laporte, K. Sivula, M. Grätzel, E. Thimsen, *Nat. Mater.* **2011**, *10*, 456.

[22] C. G. Morales-Guio, S. D. Tilley, H. Vrubel, M. Grätzel, X. Hu, *Nat. Commun.* **2014**,

5.

[23] Y. Wang, X. Yang, Q. Ma, J. Kong, H. Jia, Z. Wang, M. Yu, *Appl. Surf. Sci.* **2015,** 340, 18.

[24] X. Yang, Z. Wang, X. Lv, Y. Wang, H. Jia, *J. Photochem. Photobiol. A*. **2016**, 329, 175.

[25] X. Yang, Y. Wang, Z. Wang, X. Lv, H. Jia, J. Kong, M. Yu, *Ceram. Int.* **2016**, 42, 7192.

[26] Y. Wang, Q. Ma, H. Jia, Z. Wang, *Ceram. Int.* **2016**, 42, 10751.

[27] Y.-F. Lim, C. S. Chua, C. J. J. Lee, D. Chi, *Phys. Chem. Chem. Phys.* **2014**, *16*, 25928.

[28] C. Liu, N. P. Dasgupta, P. Yang, *Chem. Mater.* **2014**, *26*, 415.

[29] Y. Wang, T. Jiang, D. Meng, J. Yang, Y. Li, Q. Ma, J. Han, *Appl. Surf. Sci.* **2014**, 317, 414.

[30] Y. Wang, D. Wang, B. Yan, Y. Chen, C. Song, *J. Mater. Sci. Mater. Electron.* **2016**, 27, 6918.

[31] V. Figueiredo, E. Elangovan, G. Gonçalves, P. Barquinha, L. Pereira, N. Franco, E. Alves, R. Martins, E. Fortunato, *Appl. Surf. Sci.* **2008**, *254*, 3949.

[32] S. P. Meshram, P. V. Adhyapak, U. P. Mulik, D. P. Amalnerkar, *Chem. Eng. J.* **2012**, *204–206*, 158.

[33] S. Masudy-Panah, G. K. Dalapati, K. Radhakrishnan, A. Kumar, H. R. Tan, E. Naveen Kumar, C. Vijila, C. C. Tan, D. Chi, *Prog. Photovoltaics Res. Appl.* **2015**, *23*, 637.

[34] S. Masudy-Panah, K. Radhakrishnan, H. R. Tan, R. Yi, T. I. Wong, G. K. Dalapati, *Sol. Energy Mater. Sol. Cells* **2015**, *140*, 266.

[35] S. Masudy-Panah, K. Radhakrishnan, A. Kumar, T. I. Wong, R. Yi, G. K. Dalapati, *J.*

Appl. Phys. **2015**, *118*, 225301.

[36] S. Masudy-Panah, R. Siavash Moakhar, C. S. Chua, A. Kushwaha, G. K. Dalapati, *ACS Appl. Mater. Interfaces* **2017**, *9*, 27596.

[37] S. Masudy-Panah, S. Zhuk, H. R. Tan, X. Gong, G. K. Dalapati, *Nano Energy* **2018**, *46*, 158.

[38] P. Christopher, H. Xin, S. Linic, *Nat. Chem.* **2011**, *3*, 467.

[39] J. Niu, Y. Dai, L. Yin, J. Shang, J. C. Crittenden, *Phys. Chem. Chem. Phys.* **2015**, *17*, 17421.

[40] S. Anandan, G.-J. Lee, J. J. Wu, *Ultrason. Sonochem.* **2012**, *19*, 682.

[41] X. Zhang, Y. Yang, W. Que, Y. Du, *RSC Adv.* **2016**, *6*, 81607.

[42] J. Ghijsen, L. H. Tjeng, J. van Elp, H. Eskes, J. Westerink, G. A. Sawatzky, M. T. Czyzyk, *Phys. Rev. B* **1988**, *38*, 11322.

[43] W. Yao, F.-L. Li, H.-X. Li, J.-P. Lang, *J. Mater. Chem. A* **2015**, *3*, 4578.

[44] N. Padmavathy, P. K. Samantaray, L. Das Ghosh, G. Madras, S. Bose, *Nanoscale* **2017**, *9*, 12664.

[45] J. C. Klein, C. P. Li, D. M. Hercules, J. F. Black, *Appl. Spectrosc.* **1984**, 38, 729.

[46] K. Hirokawa, F. Honda, M. J. Oku, *Electron. Spectrosc. Relat. Phenom.* **1975**, 6, 333.

[47] C. C. Chusuei, M. A. Brookshier, D. W. Goodman, *Langmuir.* **1999**, 15, 2806.

[48] M. Kong, Y. Li, X. Chen, T. Tian, P. Fang, F. Zheng, X. Zhao, *J. Am. Chem. Soc.* **2011**, *133*, 16414.

[49] Y.-X. Yu, W.-X. Ouyang, Z.-T. Liao, B.-B. Du, W.-D. Zhang, *ACS Appl. Mater. Interfaces* **2014**, *6*, 8467.

[50] J. Staehelin, J. Hoigne, *Environ. Sci. Technol.* **1985**, *19*, 1206.

[51] K. D. Pickering, M. R. Wiesner, *Environ. Sci. Technol.* **2005**, *39*, 1359.

[52] C. Santaella, B. Allainmat, F. Simonet, C. Chanéac, J. Labille, M. Auffan, J. Rose, W. Achouak, *Environ. Sci. Technol.* **2014**, *48*, 5245.

[53] S. Garg, C. Jiang, C. J. Miller, A. L. Rose, T. D. Waite, *Environ. Sci. Technol.* **2013**, *47*, 9190.

Table 1. K_{app} of samples for photodegradation of ACE and TS under visible light irradiation

	ACE		**TS**	
Sample	**K_{app} (h^{-1})**	**R^2**	**K_{app} (h^{-1})**	**R^2**
As-deposited	0.06	99.17	0.138	99.6
A-CuO	0.162	98.89	0.366	99.14
Pd20-CuO	0.576	98.56	1.146	97.25
Pd40-CuO	0.796	97.12	1.81	95.25
Pd60-CuO	0.542	97.45	1.44	94.73

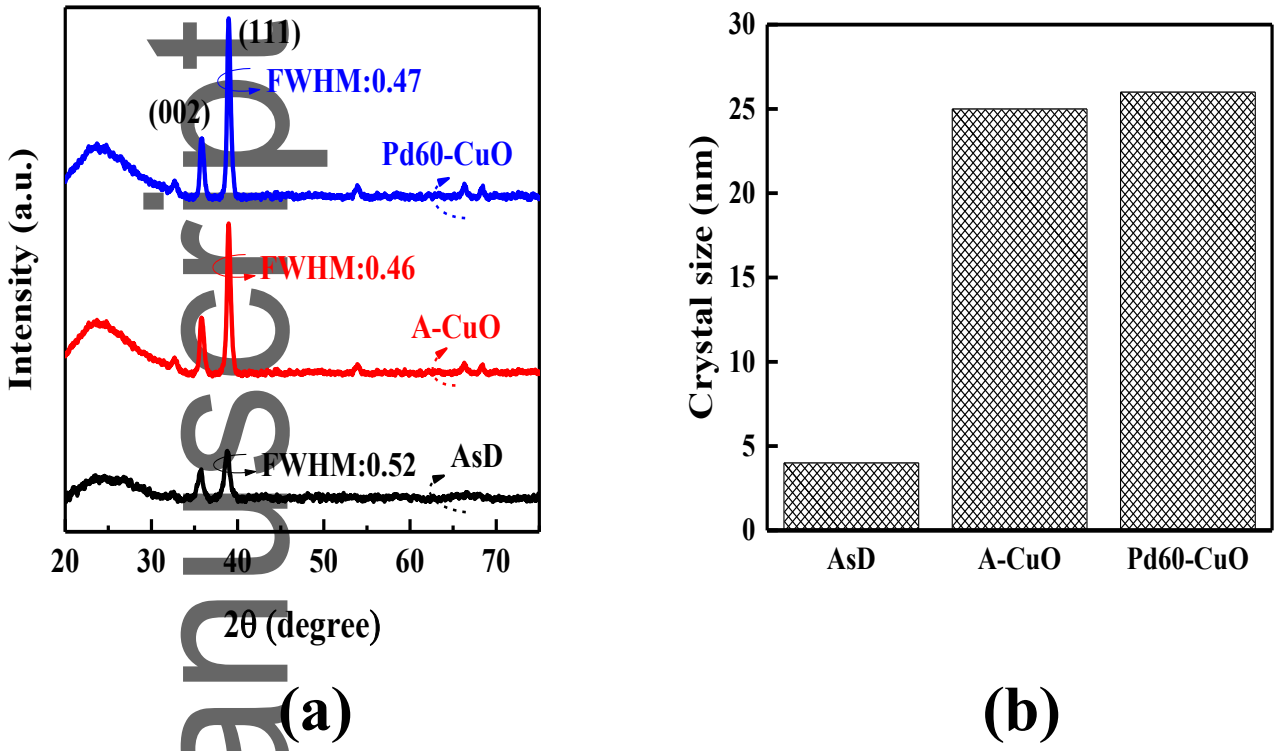

Figure 1. (a) XRD spectra of sputtered samples and corresponding FWHM of the samples (b) crystal size of samples.

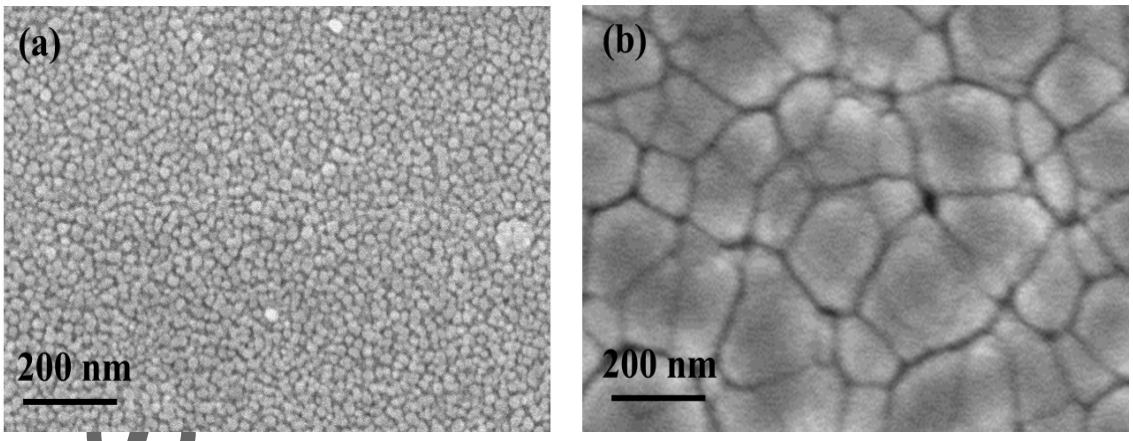

Figure 2. FESEM images of (a) As-Deposited and (b) A-CuO samples

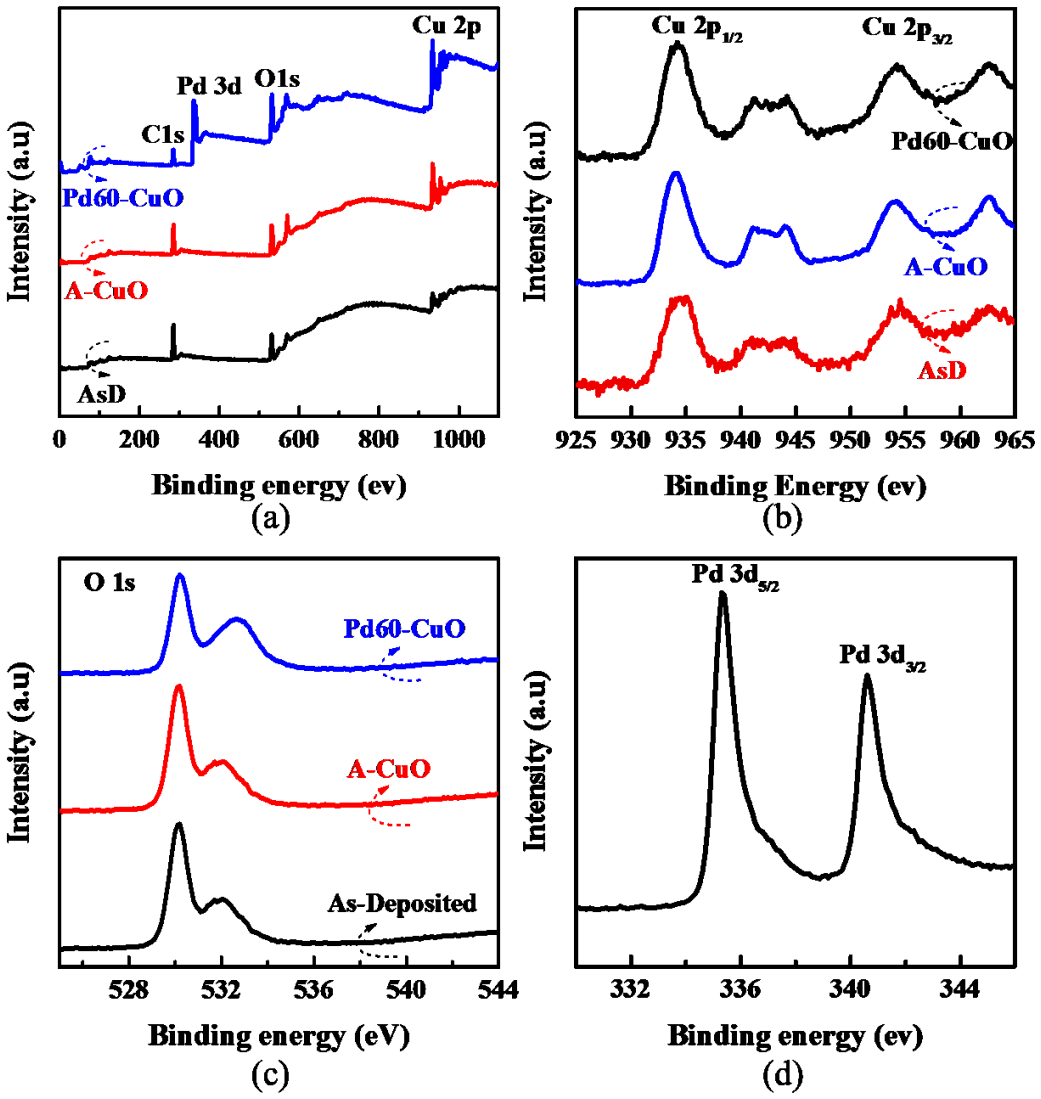

Figure 3. (a) XPS survey spectrum (b) Cu 2p , (c) O 1s of As-deposited, A-CuO and P60-CuO, and (d) Pd 3d from Pd60-CuO.

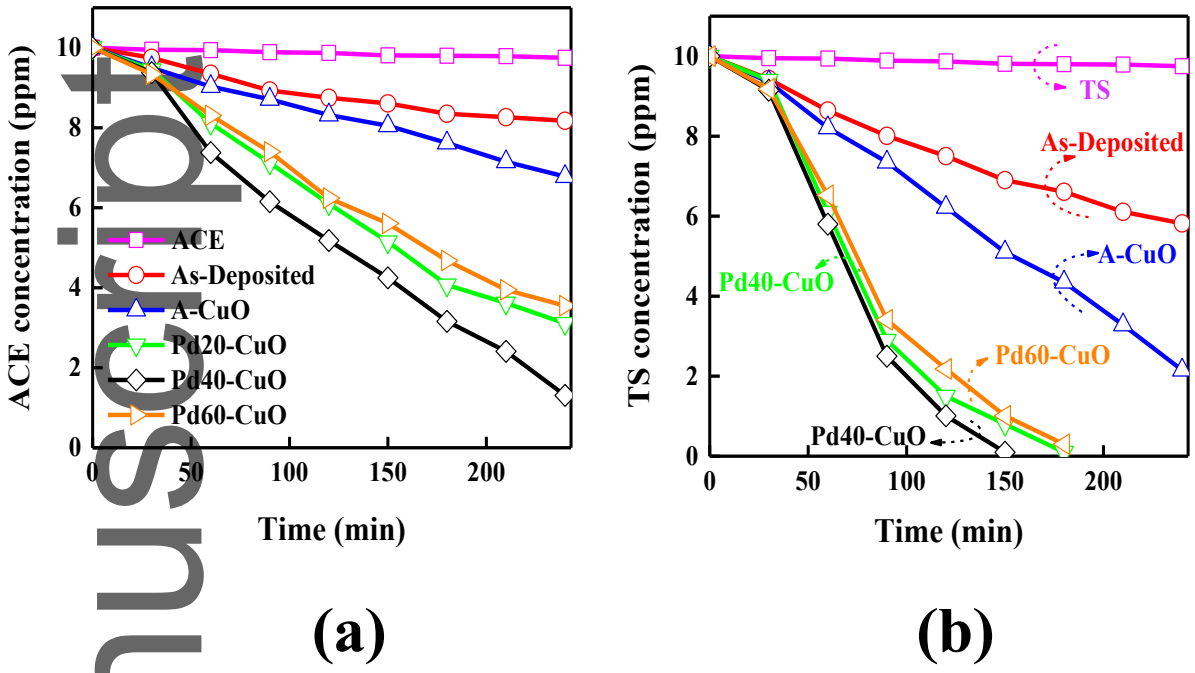

Figure 4. (a) ACE and (b) TS photocatalytic degradation under visible light irradiation (>420nm)

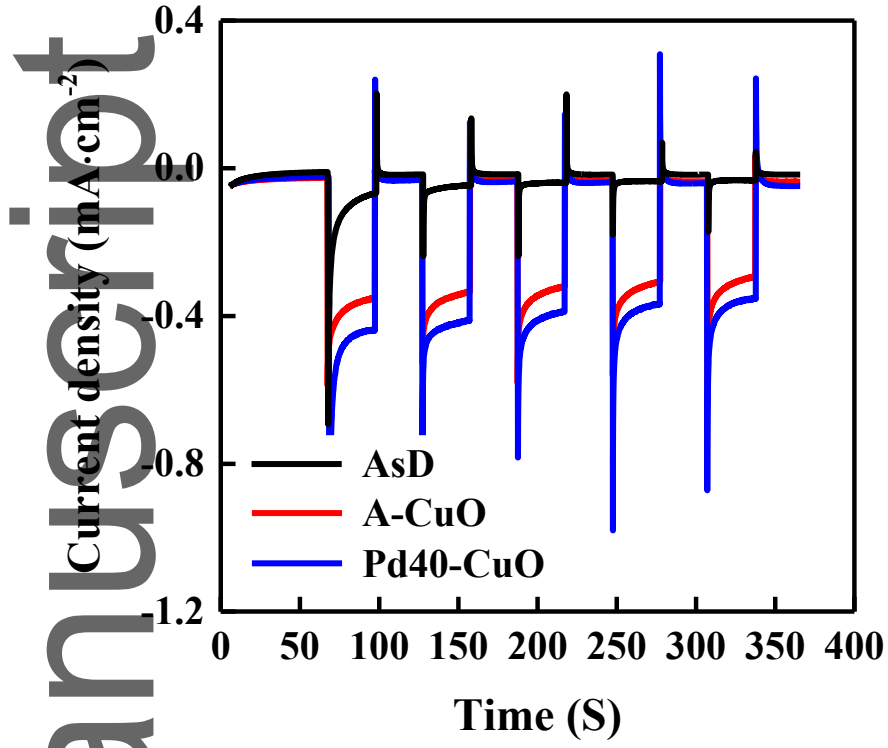

Figure 5. Photocurrent responses of As-deposited, A-CuO and Pd40-CuO under visible light illumination.

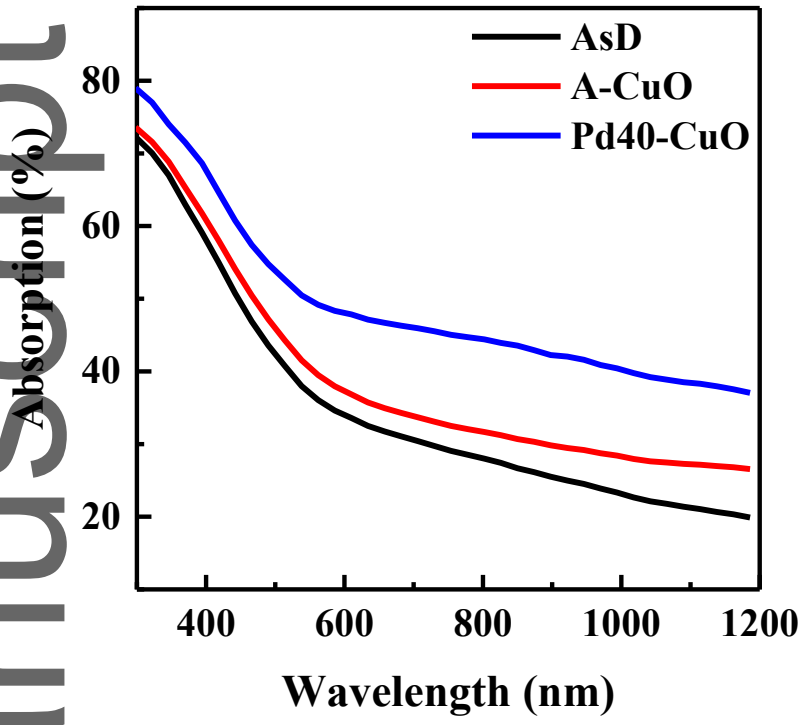

Figure 6. UV-Vis absorption spectra of As-deposited, A-CuO and Pd40-CuO.

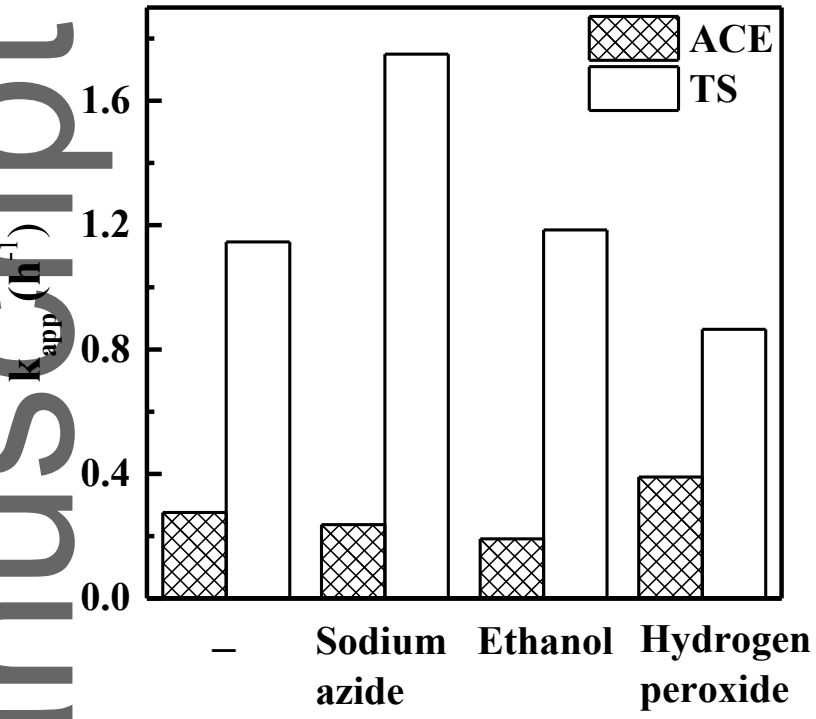

Figure 7. Effects of radical trappers on K_{app} of ACE and TS by Pd40-CuO

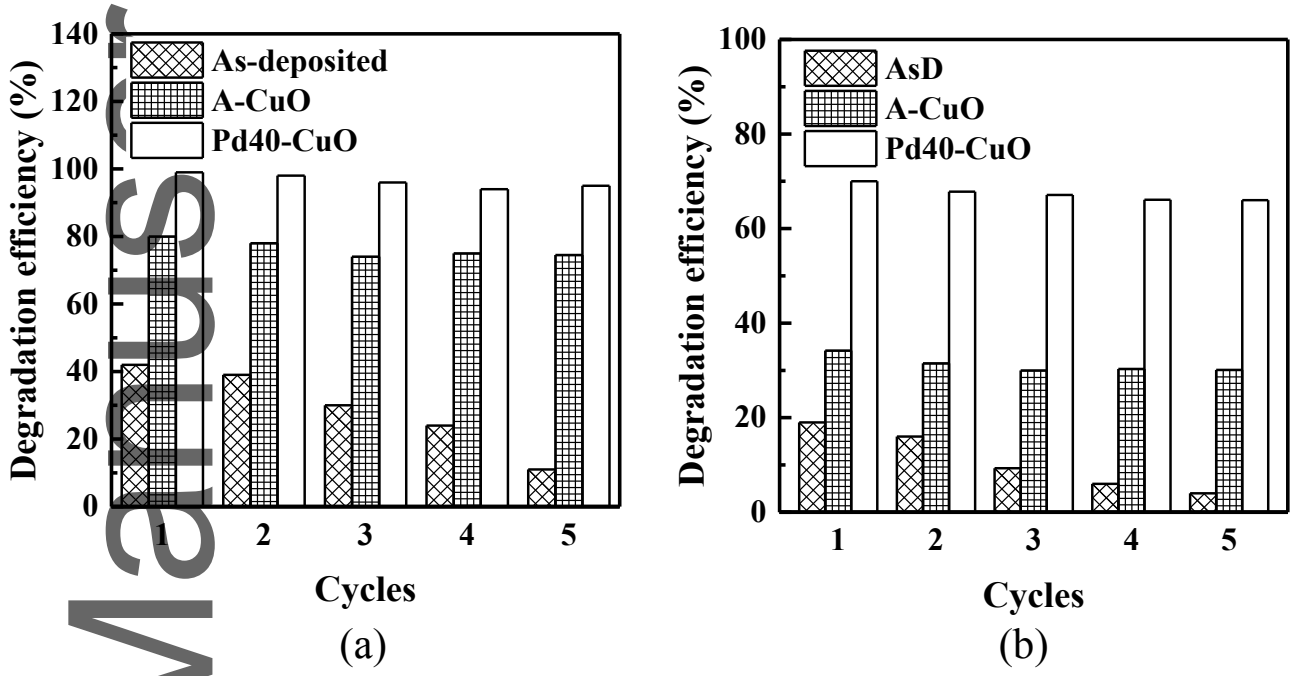

Figure 8. Recycling of As-deposited, A-CuO and Pd40-CuO for photocatalytic degradation of (a) ACE and (b) TS.

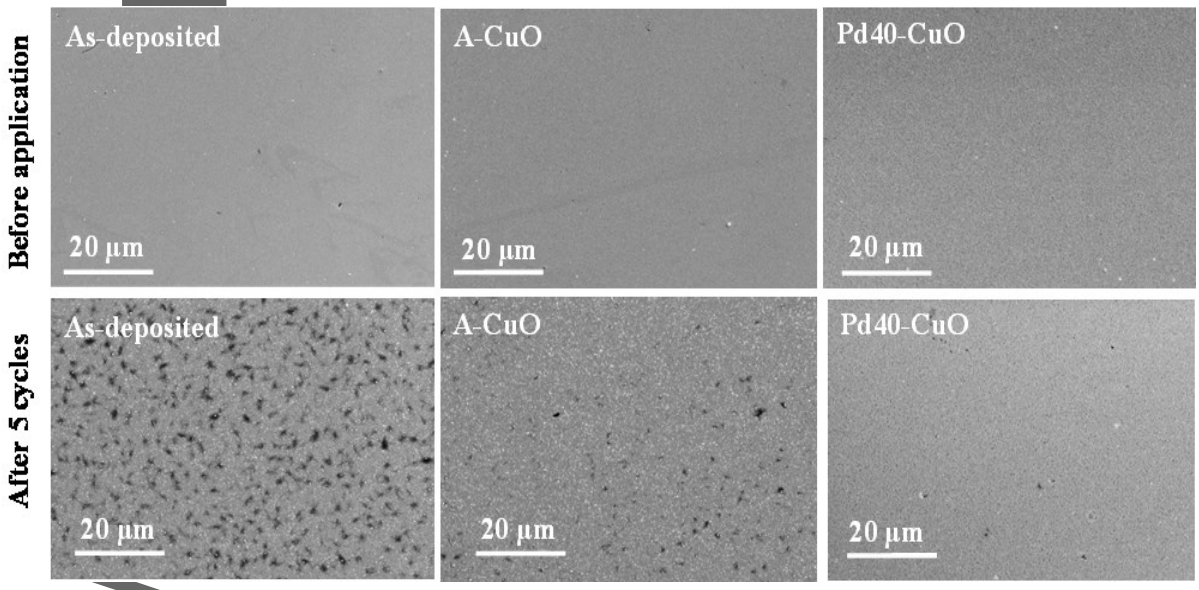

Figure 9. FESEM images of photocatalysts before and after five cycles application

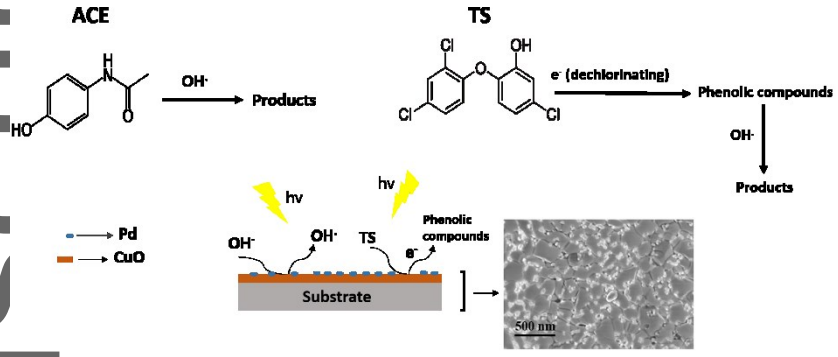

Application of Pd decorated CuO thin film for photocatalytic degradation of acetaminophen (ACE) and triclosan (TS) in aqueous solution is presented. The effect of thermal treatment on the photocatalytic activity of the CuO thin film is investigated. The photocatalytic degradation mechanism is comprehensively discussed in this article. The stability and recycling of photocatalysts are investigated.